

Tracing mass and light in the Universe: where is the dark matter?

Neta A. Bahcall and Andrea Külier*

Department of Astrophysical Sciences, Princeton University, Princeton, NJ 08544

1 November 2018

ABSTRACT

How is mass distributed in the Universe? How does it compare with the distribution of light and stars? We address these questions by examining the distribution of mass, determined from weak lensing observations, and starlight, around $> 10^5$ SDSS MaxBCG groups and clusters as a function of environment and scale, from deep inside clusters to large cosmic scales of $22 h^{-1}$ Mpc. The observed cumulative mass-to-light profile, $M/L(< r)$, rises on small scales, reflecting the increasing M/L of the central bright galaxy of the cluster, then flattens to a nearly constant ratio on scales above $\sim 300 h^{-1}$ kpc, where light follows mass on all scales and in all environments. A trend of slightly decreasing $M/L(r)$ with scale is shown to be consistent with the varying stellar population following the morphology-density relation. This suggests that stars trace mass remarkably well even though they represent only a few percent of the total mass. We determine the stellar mass fraction and find it to be nearly constant on all scales above $\sim 300 h^{-1}$ kpc, with $M_*/M_{tot} \simeq 1.0 \pm 0.4\%$. We further suggest that most of the dark matter in the Universe is located in the large halos of individual galaxies (~ 300 kpc for L^* galaxies); we show that the entire $M/L(r)$ profile — from groups and clusters to large-scale structure — can be accounted for by the aggregate masses of the individual galaxies (whose halos may be stripped off but still remain in the clusters), plus gas. We use the observed mass-to-light ratio on large scales to determine the mass density of the Universe: $\Omega_m = 0.24 \pm 0.02 \times b_{M/L}^2 = 0.26 \pm 0.02$.

Key words: galaxies: clusters: general — galaxies: groups: general — cosmology: observations — cosmological parameters — dark matter — large-scale structure of Universe

1 INTRODUCTION

Understanding the distribution of mass on large scales is a fundamental quest in cosmology. How does it compare with the distribution of stars, light, and gas? We know that individual galaxies are surrounded by large dark matter halos, and that groups and clusters of galaxies are dominated by dark matter comprising five to ten times more mass than baryonic matter (stars and gas). It is generally believed that the relative contribution of dark matter increases with scale — from galaxies, to groups, to clusters, and to large-scale structure; larger scale systems are believed to contain more dark matter, relative to light or stars, than do galaxies (Ostriker et al. 1974; Rubin et al. 1978; Davis et al. 1980; and more recently Guo et al. 2010; Leauthaud et al. 2012). In this paper we investigate the distribution of mass, light, and stars and explore how light and stars trace mass as a

function of environment and scale. We discuss the implications for the distribution of dark matter and for the stellar mass fraction.

One of the classical methods to investigate the distribution of mass in the Universe is to compare it directly with the distribution of stellar light: how does mass follow light? This method was first used on large scales by Zwicky (1937); this was followed by many additional investigations (see Bahcall et al. 1995, 2000; Carlberg et al. 1996; Sheldon et al. 2009a, and references therein). The comparison between the distribution of mass and light is represented by the mass-to-light ratio, M/L , which can be studied as a function of scale and environment. Ostriker et al. (1974), Davis et al. (1980), and others showed that M/L increases systematically with scale, from the small scale of galaxies to the larger scale of groups, clusters, and larger scale structure, indicating a growing dominance of dark matter with scale (see also Guo et al. 2010, and references therein). Bahcall et al. (1995) investigated the overall $M/L(< r)$

* E-mail: akulier@princeton.edu

function from galaxies to large scales, separating galaxies into ellipticals (older) and spirals (younger). They showed that $M/L(< r)$ rises from the small scales of galaxies up to a few hundred kpc, reflecting the large dark matter halos around galaxies, then flattens to a constant value, where light approximately traces mass, with comparable relative contribution of dark matter on all scales. Bahcall et al. (1995) thus suggest that most of the dark matter in the Universe may be located in the large dark matter halos around individual galaxies and that the dark matter in groups and clusters may simply be the sum of their individual galaxy members (plus gas). More recently, Sheldon et al. (2009a) used gravitational lensing observations of clusters from the Sloan Digital Sky Survey (SDSS) and found a similar trend of increasing M/L with radius that flattens on scales of several Mpc. The flattening of M/L on large scales indicates that light follows mass on these scales and the M/L ratio approaches a mean cosmic value (Bahcall et al. 1995, 2000; Tinker et al. 2005; Sheldon et al. 2009a).

In this paper we use the SDSS observations of weak lensing mass and the observed distribution of light around 132,473 stacked groups and clusters of galaxies at $0.1 < z < 0.3$ (Sheldon et al. 2009b; Johnston et al. 2007; Sheldon et al. 2009a) to analyze the mass-to-light profile as a function of environment, from small groups of a few galaxies to the richest clusters, and as a function of scale, from the small scale of 25 kpc inside clusters to large cosmic scales of $\sim 30 h^{-1}$ Mpc. These scales reach to $\sim 20 - 40$ virial radii of the systems, well into the large-scale cosmic environment. We investigate how light traces mass on these scales, how the M/L profile is affected by the varying stellar population, and how the stars trace the underlying mass distribution. We estimate the approximate stellar mass fraction as a function of environment and scale. We show that light and stars trace mass on scales above several hundred kpc, and that the mean stellar mass fraction is nearly constant on all these scales in all environments, $M_*/M_{tot} \simeq 1.0 \pm 0.4\%$ (§5). We further show that most of the dark matter may be located in the large halos around individual galaxies (§4).

We discuss the data in §2 and the analysis and results in §3. We investigate the contribution of individual galaxies to the total $M/L(r)$ function in §4, determine the distribution of the stellar mass fraction in §5, and calculate Ω_m in §6. We summarize our conclusions in §7. We use a flat Λ CDM cosmology with $\Omega_m = 0.27$, $\Omega_\Lambda = 0.73$, and $H_0 = 100h$ km/s/Mpc (where $h = 0.7$ should be inserted for Λ CDM; Spergel et al. 2007).

2 DATA

2.1 Cluster Sample

The MaxBCG cluster catalog (Koester et al. 2007b,a) was obtained from the Sloan Digital Sky Survey (SDSS; York et al. 2000) data release 4 (Adelman-McCarthy et al. 2006). The cluster finder is based on the red-sequence method; it maximizes the likelihood that a galaxy is a brightest cluster galaxy (BCG) at the center of an overdensity of red-sequence galaxies (Koester et al. 2007b). All clusters are selected from a 7500 deg^2 region on the sky and are in the photometric redshift range $0.1 < z < 0.3$. The cluster richness N_{200} is defined by the number of galaxies on the red

sequence with rest-frame i -band luminosity $L_i > 0.4L^*$ located within a radius r_{200}^{gals} from the BCG (where the i -band L^* is the $z = 0.1$ value from Blanton et al. 2003, corresponding to $M_* - 5 \log(h) = -20.82 \pm 0.02$, and r_{200}^{gals} is the radius within which the local galaxy overdensity is 200; see Hansen et al. 2005). The radius r_{200}^{gals} , which is used only to define the cluster richness N_{200} , differs from the r_{200} we use throughout this paper, which defines a mass overdensity of 200 times the critical density. The published catalog contains 13,823 clusters with $N_{200} \geq 10$; Sheldon et al. (2009b) (hereafter S09B) augment the catalog to include small groups of galaxies with $N_{200} \geq 3$, resulting in a sample of 132,473 groups and clusters with $N_{200} \geq 3$. The cluster photometric redshifts are accurate to 0.004, with a scatter of $\Delta z \sim 0.01$ for $N_{200} \geq 10$, degrading to $\Delta z \sim 0.02$ for the poorest systems, with the same accuracy.

2.2 Lensing Mass Measurements

The cluster sample was partitioned into 12 richness bins ranging from small groups with $N_{200} = 3$ to the richest clusters with $71 \leq N_{200} \leq 220$ (Johnston et al. 2007; hereafter J07). The number of clusters per bin decreases from 58,788 for the poorest bin to 47 for the richest. The weak lensing mass measurements were carried out by S09B and J07 on the stacked clusters in each richness bin, all centered on the cluster BCG. Because lensing is not sensitive to a uniform mass distribution (“mass sheet”), the measured mass reflects the mean mass density of the lens sample above the mean density of the Universe.

The average tangential shear of background galaxies due to lensing by the foreground stacked clusters was measured by S09B and used to calculate the mass density distribution around the clusters as a function of projected radius from the center out to scales of $30 h^{-1}$ Mpc. S09B made corrections to the density profile for contamination of the lensed sample by cluster members and residual additive biases in the tangential shear. The mass density contrast of the lensing clusters in each richness bin was measured in logarithmically spaced bins of projected clustercentric radius from $25 h^{-1}$ kpc to $22 h^{-1}$ Mpc. The 2D density contrast profile was then deprojected to a 3D density excess profile $\Delta\rho(r) \equiv \rho(r) - \bar{\rho}$ using an Abel inversion (see J07 for details). This measurement reflects the cluster-mass cross-correlation function times the mean density of the Universe, $\Delta\rho(r) = \xi_{cm}(r)\bar{\rho}$. This was used to calculate the cumulative excess mass $\Delta M(< r)$ within each radius r , as well as to find r_{200} , the radius within which the average mass density is 200 times the critical density.

We correct the mass profiles presented by Sheldon et al. (2009a) (hereafter S09A) for an improved photometric redshift distribution of the lensed background galaxies; a full description is given in §2.5.

2.3 Luminosity Measurements

The light distribution around the stacked clusters, using galaxy luminosities as defined below, was measured (by S09A) as a function of radius for the same scales as above, from $25 h^{-1}$ kpc to $30 h^{-1}$ Mpc. A uniform background was subtracted using similar measurements around random

points. The luminosity measured reflects the luminosity density of the systems above the mean, $\Delta\ell(r) = \ell(r) - \bar{\ell}$, thus representing the cluster-light cross-correlation function as a function of radius, $\Delta\ell(r) = \xi_{cl}(r)\bar{\ell}$, comparable to the mass measurements described above.

All galaxy luminosities used are in the i -band, with K -correction applied to bring them to the mean cluster redshift of $z = 0.25$; these are denoted $^{0.25}i$. All galaxy magnitudes are SDSS model magnitudes. A volume and magnitude limited sample of galaxies was chosen with $z < 0.3$ and $L_{0.25i} > 10^{9.5} h^{-2} L_{\odot} = 0.19 L_{0.25i}^* (S09A)$.

The projected luminosity profiles discussed above were inverted to obtain the 3D luminosity density profile (S09A), similar to the mass inversion. This was then integrated to obtain the excess cumulative luminosity $\Delta L(< r)$ within the same clustercentric radial bins as above, from $25 h^{-1} \text{kpc}$ to $22 h^{-1} \text{Mpc}$. Because the luminosity density was not measured within the innermost $25 h^{-1} \text{kpc}$ where the BCG is located, the average luminosity of the BCG in each stacked richness bin was added to the cumulative luminosity, so that the central L_{BCG} is included in the light (see S09A for more details).

2.4 Mass to Light Ratio

The excess mass within radius r from the center of the stacked clusters, $\Delta M(< r)$, divided by the excess luminosity within radius r , $\Delta L(< r)$, gives the mass-to-light ratio

$$\frac{\Delta M}{\Delta L}(< r) = \frac{\int_0^r dr [\rho(r) - \bar{\rho}] r^2}{\int_0^r dr [\ell(r) - \bar{\ell}] r^2} = \frac{\int_0^r dr \bar{\rho} \xi_{cm} r^2}{\int_0^r dr \bar{\ell} \xi_{cl} r^2}. \quad (1)$$

On small scales of virialized systems, this represents the mean cluster mass-to-light ratio. On large scales, as the density approaches the mean, this measures approximately the mean mass-to-light ratio of the Universe and reflects how mass traces light on large scales. A small correction factor reflecting the bias of the galaxy light tracers relative to the mass relates the observed large-scale asymptotic $\Delta M(< r)/\Delta L(< r)$ to the mean cosmic value $\langle M/L \rangle$:

$$\left(\frac{\Delta M}{\Delta L} \right)_{asym} = \left\langle \frac{M}{L} \right\rangle b_{M/L}^{-2} \\ b_{M/L}^{-2} = \frac{b_{cm}}{b_{cl}} \frac{1}{b_{\ell m}^2}. \quad (2)$$

The bias factor $b_{M/L}$ depends on the ratio of the bias of clusters relative to mass and light, b_{cm}/b_{cl} , which is near unity since the cluster bias essentially cancels out in this ratio. The bias of the galaxy tracers relative to the mass, $b_{\ell m}$, is ≈ 1 for galaxies near L^* (Sheth & Tormen 1999; Seljak & Warren 2004; Zehavi et al. 2011) and varies very slowly for galaxies below L^* (Tegmark et al. 2004; Zehavi et al. 2011). Since the luminosity threshold of the galaxy tracers is only $0.19 L^*$ (and the mean luminosity of all the galaxies within $10 h^{-1} \text{Mpc}$ is $0.65 L^*$), this implies a bias of 1.05 (for $\sigma_8 = 0.83$; Zehavi et al. 2011). Thus, on large scales, $\Delta M(< r)/\Delta L(< r)$ should approach a constant value, representing the cosmic mass-to-light ratio (with only minor bias correction).

2.5 Corrections and Uncertainties

We correct the lensing masses of J07 and S09A using the correction from Rozo et al. (2009) that reflects an improved treatment of the photometric redshift distribution of the background source galaxies based on a detailed analysis by Mandelbaum et al. (2008). This correction increases the lensing mass by $18\% \pm 2\%$ (*stat.*) $\pm 2\%$ (*sys.*). We also correct the r_{200} values by the small correction needed ($\sim 5\%$) due to this mass increase.

The mass and luminosity determinations discussed above use BCGs as the center for the stacked clusters. If the BCG is slightly offset from the center of the cluster (e.g., Niederste-Ostholt et al. 2010), both the lensing mass and luminosity in the central regions will be slightly underestimated (relative to the central mass and light of the cluster dark matter halo) although the effect will partially cancel in the mass-to-light ratio. The effect is strongest near the center of the clusters, as well as in poor groups for which miscentering is more likely to occur. However, the effect is negligible on large scales. Discussion of the effect can be found in S09A, Mandelbaum et al. (2008) and Tinker et al. (2012). We do not correct for this effect as the corrections are uncertain and are typically small (except in the poorest groups); they are not important for our main goal of understanding the behavior of the mass-to-light profile on larger scales. Our results thus reflect the mass-to-light ratio around BCG galaxies, not necessarily around the center of the dark matter halos, especially for small groups.

We further note that unless otherwise stated (e.g., §3.2-5) the luminosity accounts only for galaxies above the luminosity threshold of $L_{0.25i} > 10^{9.5} h^{-2} L_{\odot}$, as discussed above. It does not include the entire luminosity of the systems. This is discussed in §3.2.

3 ANALYSIS AND RESULTS

We combine the twelve stacked bins of groups and clusters (§2) into three broader richness bins to study the overall M/L as a function of radius around poor ($3 \leq N_{200} \leq 8$), intermediate ($9 \leq N_{200} \leq 25$), and rich ($26 \leq N_{200} \leq 220$) systems. We use the same radial bins as in S09A. We investigate both the cumulative $\Delta M(< r)/\Delta L(< r)$, and the local, differential mass-to-light profile, $\Delta m(r)/\Delta \ell(r)$. For simplicity, we refer to these as $M/L(< r)$ and $m/\ell(r)$, respectively.

The integrated mass-to-light profile $M/L(< r)$ is presented in Figure 1 as a function of radius from $25 h^{-1} \text{kpc}$ to $22 h^{-1} \text{Mpc}$ for each of the three richness bins. The observed increase of $M/L(< r)$ with radius on small scales is caused by the central BCG galaxy which dominates the cluster luminosity in the central regions (typically $\lesssim 300 \text{kpc}$): these regions reflect primarily $M/L(< r)$ of the BCG galaxy. The three top curves in Figure 1 present $M/L(< r)$ when the mean BCG luminosity is excluded from each richness bin, revealing the impact of the BCG. A comparison of the two sets of curves shows that the BCG luminosity accounts for the increasing $M/L(< r)$ in the central regions, and has negligible effect on the mass-to-light ratio on large scales. When the BCG light is excluded, the integrated mass-to-light profile is nearly flat on all scales, except for the rise on small scales that results from excluding the light (i.e., L_{BCG}) but

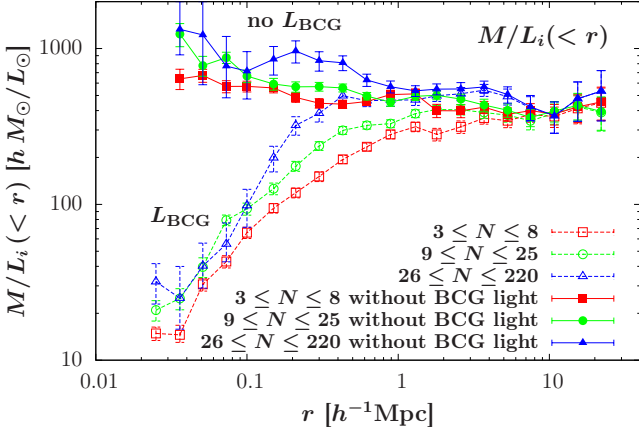


Figure 1. The cumulative mass-to-light ratio, $M/L_i(<r)$, for poor ($3 \leq N_{200} \leq 8$), intermediate ($9 \leq N_{200} \leq 25$), and rich ($26 \leq N_{200} \leq 220$) clusters. The dashed curves and related points show M/L including both the light and mass of the central BCG, whereas the solid curves and related points show $M/L(<r)$ excluding the BCG light.

not the mass. If we further exclude the mass within the central region (see below), $M/L(<r)$ flattens on all scales. On large scales $M/L(<r)$ is essentially independent of cluster richness; all environments, from the smallest groups to the richest clusters, exhibit the same overall mass-to-light ratio, reaching a universal value on scales of a few Mpc. On intermediate scales of $\sim 0.5 - 5 h^{-1}$ Mpc, while $M/L(<r)$ is nearly flat, small differences are observed as a function of richness and radius. We discuss these trends below and show that they are consistent with the varying mean stellar population age as a function of richness and radius.

The rise in $M/L(<r)$ on small scales is considerably faster for rich clusters than for poor groups (Figure 1). Rich clusters reach a nearly flat $M/L(<r)$ distribution at only $\sim 0.3 h^{-1}$ Mpc (typically near the edge of the bright BCG). Poor groups have a slow rise of $M/L(<r)$ with radius: the BCG luminosity dominates the group’s luminosity and thus $M/L(<r)$ to scales of a few Mpc. This is because the BCG luminosity, while known to increase with cluster richness ($L_{BCG} \sim M_{200}^{0.30} \sim N_{200}^{0.38}$; Hansen et al. 2009), is considerably more dominant in poor groups ($L_{BCG}/L_{200} \sim M_{200}^{-0.53} \sim N_{200}^{-0.67}$; Hansen et al. 2009). This is easily understood: in a poor group of a few galaxies, the BCG typically contains most of the group luminosity; as the group’s luminosity $\Delta L(<r)$ is integrated over radius, the BCG light dominates the group luminosity to large scales. In rich clusters, on the other hand, the BCG is brighter but constitutes only a small fraction of the total cluster luminosity at nearly all scales outside the innermost region.

Because the effect of the BCG is dominant in the innermost regions, and our interest is mostly in understanding the general behavior of $M/L(<r)$ on larger scales, we present in Figure 2 the cumulative $M/L(<r)$ profile excluding both the central BCG luminosity (as in Fig. 1) as well as the central mass. For the latter, we exclude all the mass within a central radius of $50 h^{-1}$ kpc for the poorest systems (which have the smallest BCGs) up to $150 h^{-1}$ kpc for the richest clusters. Selecting somewhat different radii for the central mass exclusion has only a small effect on the overall

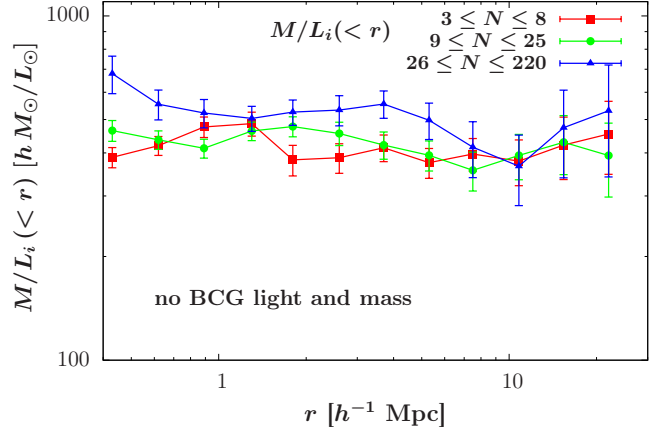


Figure 2. The cumulative mass-to-light ratio, $M/L_i(<r)$, outside the central regions, with the BCG light and central mass excluded (see §3).

$M/L(<r)$ profiles (e.g., compare with Figure 1 where no central mass has been excluded); it does not affect the main results discussed below. The $M/L(<r)$ profile outside the innermost regions (Figure 2) shows a nearly flat distribution on all scales, for all systems rich and poor, from the surprisingly small scale of few hundred kpc to the largest cosmic scales at $22 h^{-1}$ Mpc. The fact that the distribution is nearly flat on all scales indicates that stars, which make up only a few percent of the total mass, trace the distribution of mass well.

While $M/L(<r)$ is nearly flat, we observe a small trend with richness and with radius: $M/L(<r)$ increases slightly with richness at a given radius (on scales of $\lesssim 5$ Mpc), and decreases slightly with radius (up to few Mpc) for all richnesses. As we show below, these trends are consistent with the different mix of stellar populations — old in E/S0 galaxies and younger in spiral galaxies — as a function of radius and richness. Following the density-morphology relation (Dressler 1980; Dressler et al. 1997; Postman & Geller 1984; van der Wel 2008; Bamford et al. 2009), the fraction of E/S0 galaxies is high in high-density regions (rich clusters), and decreases with radius and richness to the lower density regions on larger scales and in poorer groups. Since early-type galaxies are dominated by an old stellar population with negligible recent star formation, their M/L_i ratio is larger (by a factor of ~ 2 ; see below) than that of the younger stellar population of spiral galaxies, whose luminosities are dominated by bright young stars. As the fraction of spirals increases with radius, the integrated M/L of the cluster decreases slowly with radius, as observed. The small increase of M/L from poor to rich clusters at a given radius (Figure 2) reflects partly the same effect: at a given radius a more massive cluster is generally at a smaller multiple of its virial radius, and thus a higher density, so it is dominated by a larger fraction of old E/S0s with higher M/L .

Figures 3 and 4 present the cumulative and local (differential) mass-to-light profiles, respectively, as a function of radius in units of the physical scale of the system, r/r_{200} , from small scales to nearly $40r_{200}$. In Figure 3, we again exclude the BCG luminosity and the innermost mass in order to better understand the overall trend of $M/L(<r)$ without

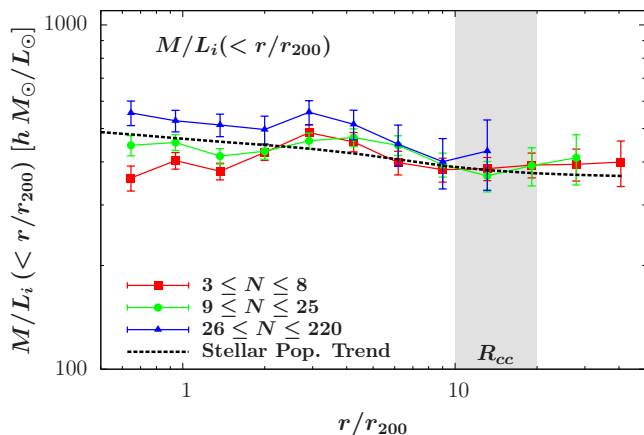


Figure 3. The cumulative mass-to-light ratio, $M/L_i(< r)$, outside the innermost cluster regions (BCG mass and light excluded). Same as Figure 2, but plotted against the clustercentric radius in units of r_{200} . The dashed line shows the expected trend of the varying stellar population age as a function of scale (§3). The vertical band shows the location of the group and cluster correlation scale.

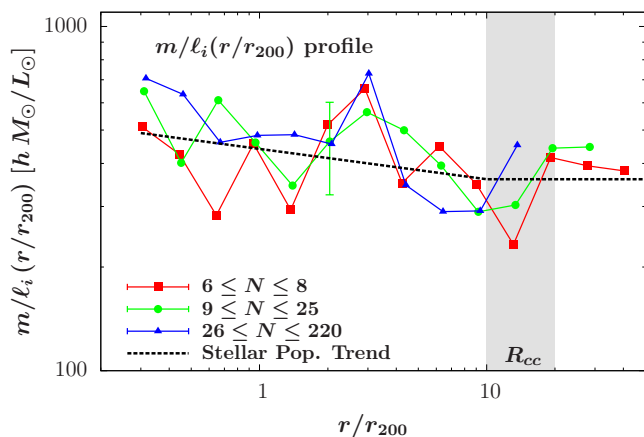


Figure 4. The local mass-to-light profile, $m/l_i(r)$, plotted against the clustercentric radius in units of r_{200} . The dashed line shows the expected trend of the varying stellar population (see text). For clarity, only a representative error bar is shown.

the dominant impact of the BCG. The differential analysis (Figure 4) is independent of the BCG, except in the very central region, since it reflects the local $m/l(r)$ ratio at any radius. The results in both figures highlight the similarity of $M/L(r/r_{200})$ for all systems and on all scales. Mass and light appear to follow each other — especially when accounting for the stellar population age — from deep inside clusters (outside their BCG cores) out to large cosmic scales.

Figure 5 presents the observed profiles of the mass density, luminosity density, and galaxy number density for all environments as a function of r/r_{200} . The profiles are nearly identical, independent of richness. This similarity of profiles is equivalent to the similar $m/l(r)$ profile observed for all systems as shown above. Since r/r_{200} corresponds to a similar overdensity for all systems, no significant stellar population effect is expected between the different richness bins, and none is observed.

The richest clusters show a slightly higher cumulative $M/L(< r)$ at $r/r_{200} \lesssim 4$ (Figure 3). This is caused by a somewhat higher M/L at the very center of the clusters, which may reflect a higher central mass concentration relative to luminosity in the innermost regions of the richest systems (e.g., more massive or extended BCGs than our central mass exclusion and/or loss of luminosity due to merging).

The $m/l(r)$ profile (Figure 4) is similar for all richness groups and on all scales starting from deep inside clusters ($r \sim 0.3r_{200}$); the profile decreases slowly with radius, by a factor of ~ 1.5 , from small scales up to several r_{200} and remains flat thereafter to nearly $40r_{200}$. This trend is consistent with the stellar population mix, which we quantify below.

We use the mean observed relative stellar M_*/L_i ratio of early-type versus spiral galaxies of $(M_*/L_i)_E/(M_*/L_i)_S \simeq 2$ (Kauffmann et al. 2003; Bell et al. 2003; Blanton & Roweis 2007; Yoshino & Ichikawa 2008; Gallazzi & Bell 2009; Leauthaud et al. 2012). This is consistent with Bruzual & Charlot (2003) single stellar population synthesis models with ages 10 Gyr versus 4 Gyr, the approximate mean ages of stellar populations in E/S0 and spiral galaxies (albeit with much scatter; see Trager et al. 2000; Proctor & Sansom 2002; Thomas et al. 2005; Kuntschner et al. 2010; Zhu et al. 2010; Roediger et al. 2011). We combine this ratio with the mean fraction of early and late type galaxies using the density-morphology relation discussed above. Here we use a typical E/S0 fraction of 40% on large-scales ($> 10r_{200}$), increasing to 90% in the central high-density regions of groups and clusters ($< 0.4r_{200}$). The resulting mass-to-light ratio then decreases by a factor of ~ 1.4 from the centers of clusters to the lower densities on large scales. This is presented by the dashed lines in Figures 3 and 4 (for the cumulative and differential functions, respectively). This expected trend agrees well with the observed M/L profile for all systems, suggesting that the small decline in M/L as a function of scale can be accounted for by the different stellar population. Clusters have a strong spatial auto-correlation function and are located in high-density regions with a higher density of older galaxies that extends to large scales; this is likely the reason that the high $m/l(r)$ ratio persist to several r_{200} before dropping to a lower more constant field value on large scales. The typical cluster correlation scale is $\sim 10 - 20r_{200}$ (Bahcall et al. 2003) for both poor and rich clusters; this is shown by the vertical band in Figures 3 and 4. While M/L reaches the cosmic value on these large scales, we emphasize that when the stellar population age is accounted for, all systems exhibit the same mean mass-to-light ratio on all scales. Light, or more precisely stellar mass, thus traces the total mass remarkably well on nearly all scales. This is discussed further in §5.

An alternate way to view the behavior of $M/L(< r)$ for different environments and scales is presented in Figure 6. Here we show $M/L(< r)$ as a function of mean cluster luminosity within r_{200} (a proxy for cluster richness or mass), for several radii; this is an inverse of the previous plots of $M/L(< r)$ presented for a few richness groups. Figure 6 shows the direct dependence of $M/L(< r)$ on the richness (mass) of the central environment. The cumulative $M/L(< r)$ is presented within two radii, $3.1 h^{-1} \text{ Mpc}$

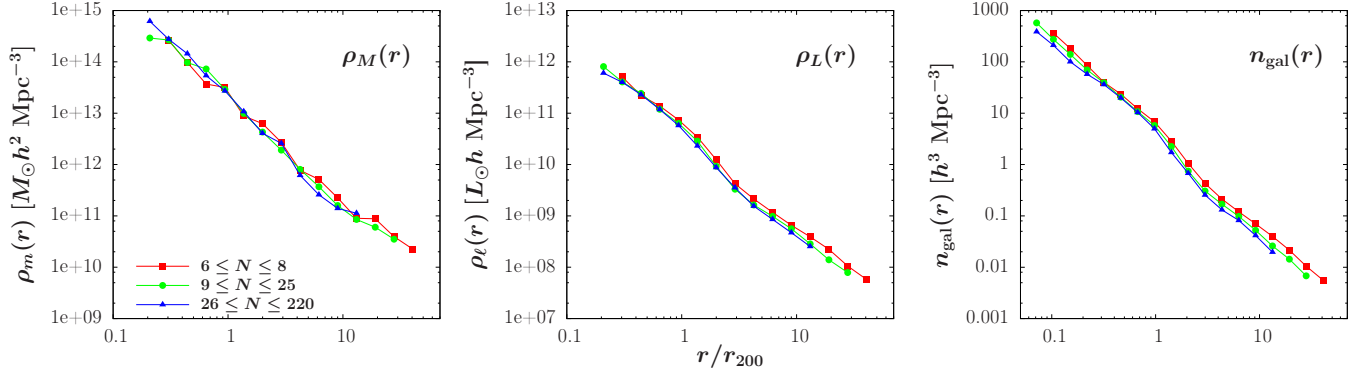


Figure 5. The density profiles of mass, $\rho_m(r)$, luminosity $\rho_\ell(r)$, and galaxy number density $n_{\text{gal}}(r)$ as a function of r/r_{200} for clusters of different richnesses. (The $n_{\text{gal}}(r)$ plot has a slightly different horizontal axis scaling.)

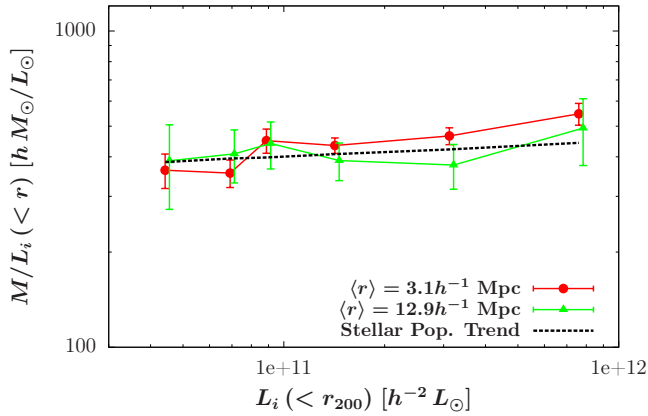


Figure 6. The cumulative mass-to-light ratio, $M/L_i(<r)$, as a function of the mean cluster luminosity within r_{200} , $L_i(<r_{200})$ (a proxy for cluster richness or mass). The mass-to-light ratio is shown within two radii, $3.1 h^{-1}$ Mpc and $12.9 h^{-1}$ Mpc. The dashed line represents the expected trend of the varying stellar age (for $\sim 3.1 h^{-1}$ Mpc; see text). The BCG mass and light are excluded.

and $12.8 h^{-1}$ Mpc. The mass and light of the central BCG have been excluded in Figure 6 as they were in Figures 2 and 3, although the effect of the BCG is negligible on the larger scale (~ 12.9 Mpc). Each point in the cluster luminosity $L_i(<r_{200})$ is an average of two of the twelve original richness bins. The stellar population effect as a function of $L_i(<r_{200})$ for the 3.1 Mpc radius is shown by the dotted line; it agrees well with the observed M/L function, except for the richest clusters, which as described above contain an increased amount of mass compared to light at their very centers. Here, the slow increase of M/L with richness due to the stellar population trend is caused by the fact that the same physical radius corresponds to a different galaxy overdensity in environments of different richness.

Figure 7 presents the integrated $M/L(<r)$ versus luminosity (richness) for all systems within the large scales of 9 and $18.4 h^{-1}$ Mpc. The M/L contains all the mass and light including that of the BCG. The integrated $M/L(<r)$ ratio on these scales is constant, independent of the central environment; the mass-to-light ratio reaches a mean cosmic value of $409 \pm 23 h M_\odot/L_\odot$. As seen in the previous figures, the

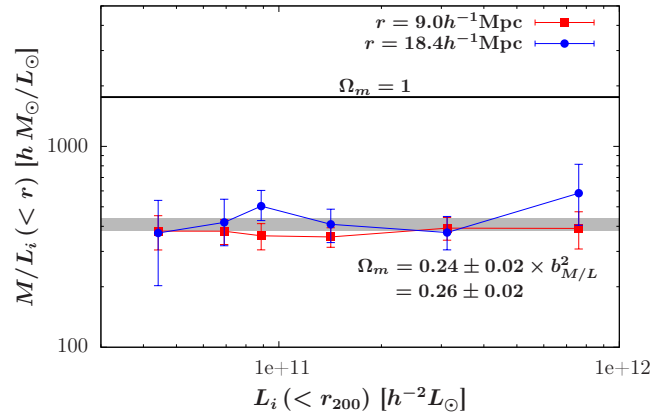


Figure 7. $M/L_i(<r)$, including the BCG mass and light, as a function of richness at large scales ($9.0 h^{-1}$ Mpc and $18.4 h^{-1}$ Mpc). The horizontal axis is $L_i(<r_{200})$, the cumulative light within r_{200} , a proxy for the cluster richness or mass. M/L is constant on these scales, independent of the central environment. The gray band shows the mean $\langle M/L_i \rangle = 409 \pm 29 h M_\odot/L_\odot$. This corresponds to a cosmic mass-density of $\Omega_m = 0.24 \pm 0.02 b_{M/L}^2 = 0.26 \pm 0.02$ (see §6).

same constant value is reached even within the inner parts of clusters when the stellar population is accounted for.

3.1 Discussion of The Mass to Light Function

All the measurements discussed above are centered on the BCG, which may be slightly offset from the center of the dark matter halo of the cluster. Our results therefore reflect the distribution of M/L around BCGs out to large cosmic scales and should be so interpreted. Furthermore, for scales outside the innermost regions of clusters, the possible miscentering has negligible impact on M/L . The poorest groups have the highest uncertainty in terms of cluster centering, luminosity uncertainties (S09A), and mass uncertainties because of the weaker lensing signal. Therefore, the poorest groups ($N \lesssim 9$) are prone to larger uncertainties.

Previous results found that $M/L(<r_{200})$ increases with cluster richness (mass), approximately as $M/L(<r_{200}) \sim M_{200}^{0.2-0.3}$ (e.g., Girardi et al. 2000; Bahcall & Comerford 2002; Lin et al. 2004; Popesso et al. 2007; Sheldon et al.

2009a). Here we show that this is mostly the effect of the BCG luminosity: the r_{200} scale of the poorest groups is nearly the same size as the BCG galaxy (a few hundred kpc), therefore the group $M/L(< r_{200})$ is dominated by the lower $M/L(< r)$ of the BCG, while the BCG luminosity of rich clusters is negligible at the cluster scale of $r_{200} \sim 1$ Mpc. Using the observed relations ($L_{BCG} \propto M_{200}^{0.3}$ and $L_{BCG}/L_{200} \sim M_{200}^{-0.53}$; §3; Hansen et al. 2009) we find $M/L(< r_{200}) = M_{200}/L_{200} \sim M_{200}^{0.2}$, as is indeed observed. Comparing the M/L profile outside the innermost region (at $r/r_{200} \gtrsim 0.3$), we show that $M/L(r/r_{200})$ is nearly independent of richness (Figures 3 and 4). The nearly flat distribution of $M/L(r)$ persists on all scales, from $r \sim 0.3r_{200}$ (~ 80 kpc in small groups and ~ 300 kpc in large clusters) out to nearly $30 h^{-1}$ Mpc. The small decrease in the mass-to-light ratio as a function of r/r_{200} is consistent with a decreasing stellar population age as a function of local galaxy density (§3). This effect, combined with the fact that the physical radius r corresponds to a different galaxy density in clusters of different richnesses, also accounts for the observed trend in $M/L(< r)$ as a function of cluster richness at fixed r (Figure 6). This agreement implies that the underlying mass and light distribution, when accounting for the stellar population age, follow each other remarkably well on all scales. It further suggests that the stellar mass fraction, M_*/M , is nearly constant on these scales (see §5).

3.2 Total Luminosity

The luminosities discussed above do not represent the total luminosities since they include only galaxies above the threshold of $L_i^{0.25} = 10^{9.5} h^{-2} L_\odot = 0.19 L_{0.25}^*$ (§2). The luminosity contributed by fainter galaxies is not included, and neither is the diffuse intracluster light (ICL) — integrated light from individual stars in the cluster potential (Zibetti et al. 2005). While this does not affect the self-consistent results discussed above, the total luminosity should be accounted for when comparing our results with other measurements. We estimate these additional luminosities contributions below.

Galaxies below the threshold of $10^{9.5} h^{-2} L_\odot = 0.19 L^*$ are estimated to contribute an additional 36% to the current luminosity, using the observed Schechter luminosity function of SDSS galaxies which has a faint-end slope of -1.21 in the i -band (S09A; consistent with Montero-Dorta & Prada 2009 and Blanton et al. 2001). The radial distribution of faint galaxies is assumed to be similar to that of the other galaxies as suggested by the SDSS observations of Hansen et al. (2009) showing that the galaxy luminosity function in groups and clusters is independent of radial scale.

The diffuse intracluster light (ICL) from individual stars, thought to be stripped from galaxies as a result of gravitational interactions within groups and clusters, has been measured in detail for SDSS clusters at $z \approx 0.25$. Zibetti et al. (2005) used stacked images of 683 clusters to measure the ICL in the i -band out to 700 kpc. They find that the ICL contributes $\sim 11\%$ of the luminosity in groups and clusters, nearly independent of cluster richness and BCG luminosity. The ICL is more concentrated than the galaxy distribution. Tal & van Dokkum (2011) measure the ICL around 42,000 stacked SDSS Luminous Red Galaxies (LRGs) that are located in the centers of groups and clus-

ters. They find an ICL contribution of $\sim 20\%$. We adopt an ICL correction of 15% additional luminosity (i.e., $\sim 13\%$ of the total cluster luminosity).

We add the above luminosity of faint galaxies (36%) and the intracluster light (15%); they decrease the M/L ratios by these factors (1.36 and 1.15) on the group and cluster scales (i.e., $< r_{200}$), and by 36% (a factor of 1.36) everywhere else. This corrected total $m/\ell(r)$ profile is presented in Figure 8. It enables us to compare the results with other measurements and with the contribution from individual galaxies, as discussed in §4.

4 MASS TO LIGHT CONTRIBUTION FROM INDIVIDUAL GALAXIES

It is generally believed that groups and clusters have significantly more dark matter (relative to light) than individual $\sim L^*$ galaxies (e.g., Ostriker et al. 1974; Davis et al. 1980; Guo et al. 2010). Bahcall et al. (1995) and Bahcall & Fan (1998) suggested, however, that clusters and groups do not contain significantly more dark matter per unit light than do galaxies, but instead most of the dark matter resides in the large halos of individual galaxies; these make up the dark matter observed in groups, clusters, and large-scale structure. We investigate this further below: how much of the observed mass, and thus M/L , is contributed by individual galaxies (plus gas). We use the mean observed mass-to-light ratio of typical isolated $\sim L^*$ elliptical and spiral galaxies, combined with the density-morphology relation (§3) to estimate the amount of mass and M/L contributed by individual galaxies to the observed M/L profile on all scales and in all environments.

As discussed in §3, the $M/L(< r)$ function flattens to a constant value at approximately $\sim 300 h^{-1}$ kpc. This scale is comparable to the virial radius of bright L^* galaxies ($\sim 250 - 300 h^{-1}$ kpc at the virial overdensity of $\sim 95\rho_c$ relevant for Λ CDM). If galaxy halos extend to these scales, as suggested by observations (below), could the dark matter of individual galaxies (including these large halos), plus the known gas component, account for all or most of the mass observed in the $M/L_i(< r)$ function, from small scales inside clusters to the large cosmic scales of nearly $30 h^{-1}$ Mpc? To test this we use, for simplicity, a $\sim 300 h^{-1}$ kpc halo radius around L^* galaxies, with M/L_i values that are consistent with observations: $M/L_i(\lesssim 300 h^{-1}) \sim 150 h M_\odot/L_\odot$ for spirals, and, with a factor of two lower L_i for older galaxies (§3), an $M/L_i(\lesssim 300 h^{-1}) \sim 300 h$ for early-type L^* galaxies (E/S0).

These values are motivated by observations of individual L^* galaxies. For example, the Milky Way (MW) and M31, both nearly L^* spiral galaxies, have been measured in detail to determine their extended masses (see below). Their luminosities are $L_i(\text{MW}) \sim 3 \times 10^{10} L_\odot$ and $L_i(\text{M31}) \sim 3.5 \times 10^{10} L_\odot$ (Cox 2000 observe $L_B(\text{MW}) = 2.4 \times 10^{10} L_\odot$; Courteau & van den Bergh 1999 infer $M_V(\text{MW}) = -20.9$ and $M_V(\text{M31}) = -21.2$; Flynn et al. 2006 report $L_I(\text{MW})$ in the range $3 - 4 \times 10^{10} L_\odot$; Tamm et al. 2012 find a total M31 luminosity of $3.5 \times 10^{10} L_\odot$). This luminosity is consistent with the SDSS L_i^* used above ($3.3 \times 10^{10} L_\odot$ when converted to $h = 0.7$).

The extended mass of the Milky Way and M31 have

been measured recently using proper motions observed with the Hubble Space Telescope (HST) combined with the Timing Argument (TA); van der Marel et al. (2012) determine the sum of the two virial masses to be $4.93 \pm 1.6 \times 10^{12} M_{\odot}$, consistent with the Li & White (2008) revised TA method that gives $5.27 \pm 0.5 \times 10^{12} M_{\odot}$. Boylan-Kolchin et al. (2013) combined the Leo-I proper motion with the TA method and other measurements to obtain $M(MW) \sim 1 - 2.4 \times 10^{12} M_{\odot}$, and Li & White (2008) obtain an estimated virial mass of $M(MW) \sim 2.4 \times 10^{10} M_{\odot}$. More recently, Phelps et al. (2013) applied the Least Action Method (Peebles 1989) to the local group galaxies to derive masses that are consistent with the high end of the above values: they find $M(MW) = 2.5 \pm 1.5 \times 10^{12} M_{\odot}$ and $M(M31) = 3.5 \pm 1 \times 10^{12} M_{\odot}$; their best value for the MW increases to $M(MW) = 3.5 \pm 1.5 \times 10^{12} M_{\odot}$ when data of four external groups is included. Considering the above masses and luminosities, while uncertain, we use as approximate values $M/L_i \sim 100(h = 0.7) \approx 150h M_{\odot}/L_{\odot}$ for $\sim L^*$ spiral galaxies (within radius $\sim 250 - 300$ kpc). Early-type galaxies, with their fainter L_i luminosities (by a factor of about 2), thus imply $M/L_i (\lesssim 300 h^{-1} \text{ kpc}) \sim 200(h = 0.7) M_{\odot}/L_{\odot} \approx 300h M_{\odot}/L_{\odot}$ for $\sim L^*$ E/S0 galaxies. This is consistent with recent observations of isolated early-type galaxies using weak and strong gravitational lensing. Lagattuta et al. (2010) use HST data to study strong and weak lensing by isolated elliptical galaxies and find a mean $M/L_V (\lesssim 300 h^{-1} \text{ kpc}) = 300 \pm 90h$, consistent with the value above. Brimiouille et al. (2013) conduct a detailed weak-lensing analysis of galaxies from the CFHT Legacy Survey, finding a mean $M/L_r \sim 287_{-95}^{+95}h$ for red L^* galaxies in low-density regions (using a truncated isothermal sphere model with an observed best-fit truncation radius of $245_{-52}^{+64} h^{-1} \text{ kpc}$). They also find a mean $M/L_r \sim 178 \pm 22h$ for all the red and blue galaxies combined (with a best-fit truncation radius of $184 h^{-1} \text{ kpc}$).

We adopt the above $M/L_i(\text{E/S0}) \sim 300h M_{\odot}/L_{\odot}$ and $M/L_i(\text{Sp}) \sim 150h M_{\odot}/L_{\odot}$ within ~ 300 kpc of individual $\sim L^*$ galaxies as approximate values to illustrate the contribution of galaxies to the dark matter and $M/L(< r)$ function on all scales. To determine how much galaxies with these M/L_i ratio contribute we combine these galaxy M/L_i values with the density-morphology relation that describes the mean observed fraction of spiral and E/S0 galaxies as a function of density (§3). The E/S0 fraction decreases from nearly $\sim 90 - 100\%$ at the high-density regions of clusters to $\sim 40\%$ in the low-density field on large scales. This yields an estimate of the mean M/L_i contributed by the galaxies. (We note that while the large dark matter halos of individual galaxies may be stripped off in the dense regions of clusters, and halos may overlap, the total mass remains within the cluster potential.) The contribution from galaxies therefore ranges from $M/L_i \sim 270 - 300h$ in the dense regions of clusters, decreasing to $\sim 210h$ on large scale (where $\sim 40\%$ of galaxies are E/S0s). We add the additional gas component that exists on all scales; for this, we use a gas component that is $\sim 15\%$ of the total mass, since the cosmic baryon fraction is 17% (Spergel et al. 2007), and the stellar fraction is $\sim 1 - 2\%$ (§5). This is consistent with the extended gas distribution observed in groups and clusters within their virial radii (Rasheed et al. 2010). Using a lower gas fraction, as observed in the central parts of small groups ($< r_{500}$), or a slightly varying gas fraction, only affects the

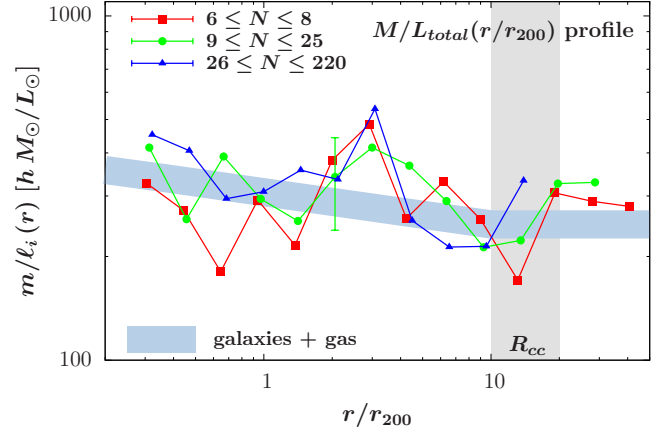


Figure 8. The mass-to-light profile, where L_{total} is the total luminosity (including light from faint galaxies below our luminosity threshold plus the diffuse ICL; see §3.2). The declining blue band represents the M/L of individual galaxies plus gas (§4). The galaxies plus gas appear to contribute all or most of the total observed $M/L(r)$ function on all scales and environments.

results on the smallest scales ($r/r_{200} < 0.7$) of small groups by $\lesssim 10\%$, well consistent with the observed $M/L(r)$ function. On larger scales, the intergalactic medium (IGM) is expected to contain a similar gas fraction (Cen & Ostriker 2006; see also Prochaska et al. 2013 for the extended gas component observed in the circumgalactic medium around galaxies).

This sum of galaxy and gas mass represents the mass contributed by individual galaxies (including their dark matter halos) plus the intracluster/intergalactic/circumgalactic gas. This contribution ranges from $M/L_i \sim 340h$ inside rich clusters, decreasing to $\sim 250h$ on large scales. This M/L_i of individual galaxies plus gas is plotted as the declining blue band in Figure 8. It agrees remarkably well with the entire observed $m/\ell_i(r/r_{200})$ profile — from the small scales inside groups and clusters to the largest cosmic scales of nearly $30 h^{-1}$ Mpc.

The comparison in Figure 8 shows that individual galaxies and their large dark matter halos, plus the intracluster/intergalactic gas, can account for all or most of the mass in groups, clusters, and on large scales, reproducing both the total amount of dark matter and the overall distribution of mass and light on all scales. This suggests that most of the dark matter in the Universe may be located in the large halos of individual galaxies; groups, clusters, and large-scale structure do not appear to contain significantly more dark matter (relative to light) than do their L^* galaxy members. This is consistent with the earlier results of Bahcall et al. (1995).

The values used above for individual galaxies are approximate, with large uncertainties. Using lower M/L_i values for galaxies will reduce their contribution, and vice versa. Faint galaxies, which are known to have higher M/L ratios, will further increase the dark matter contribution from individual galaxies.

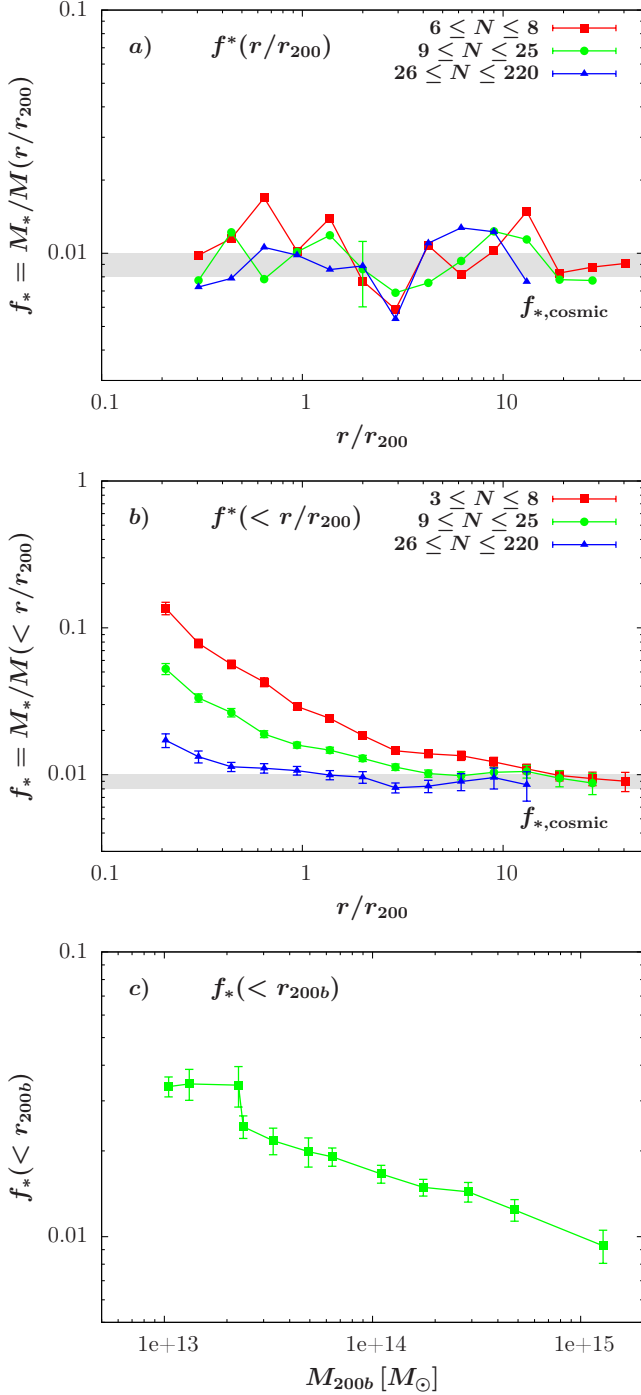


Figure 9. *a*) The local stellar mass fraction $f_*(r) = M_*/M(r)$ as function of r/r_{200} , for the three richness bins. The horizontal band shows the cosmic stellar mass fraction (§5). *b*) As in panel *a*, but for the cumulative stellar mass fraction $f_*(< r)$. *c*) The stellar fraction f_* within r_{200b} (the radius within which the mean density is 200 the matter density) plotted as a function of M_{200b} (the mass within r_{200b}).

5 STELLAR MASS FRACTION

The nearly flat distribution of M/L_i with radius, especially when accounting for the age of the stellar population, suggests that the stellar mass fraction may be similar in all environments, thus causing light to trace mass. We estimate below the implied stellar mass fraction as a function of scale and environment. We divide the mean observed stellar mass-to-light ratio M_*/L_i of early and late-type galaxies, coupled with their relevant fraction as given by the density-morphology relation (§3), by our M/L_i , including the BCG. This yields the approximate stellar mass fraction $f_* = M_*/M$:

$$f_*(r/r_{200}) = M_*/M(r/r_{200}) \quad (3)$$

$$\simeq \left[\frac{M_*/L_i}{M/L_i}(\text{E/S0, S}) \right] (r/r_{200})$$

Estimates of the M_*/L_i ratios of E/S0s and spirals vary significantly throughout the literature, although most stellar and dynamical mass-to-light estimates yield $(M_*/L_i)_E/(M_*/L_i)_S \simeq 2$ (Kauffmann et al. 2003; Bell et al. 2003; Blanton & Roweis 2007; Yoshino & Ichikawa 2008; Gallazzi & Bell 2009; Leauthaud et al. 2012). Stellar mass-to-light ratio determinations can differ as a result of the precise stellar population synthesis model and data used to obtain them. Graves & Faber (2010) compare several M_*/L_V estimates for early-type galaxies from different sources, all corrected to $z = 0$ and a Chabrier initial mass function (IMF) for consistency. A similar comparison for M_*/L_I (G. Graves, private communication) reveals that models based on fits to observational spectra (Kauffmann et al. 2003, using SDSS data; Gallazzi et al. 2005) give $M_*/L_I(\text{E/S0}) \simeq 2.5M_\odot/L_\odot$ (and $M_*/L_I(\text{Sp}) \simeq 1.3M_\odot/L_\odot$), as does a single burst star formation model. Models based on fits to photometric SEDs (Bell et al. 2003; Blanton & Roweis 2007) find lower values of $M_*/L_I(\text{E/S0}) \simeq 2M_\odot/L_\odot$ ($M_*/L_I(\text{Sp}) \simeq 1M_\odot/L_\odot$). Similarly, Leauthaud et al. (2012), using the COSMOS data, find $M_*/L_i(\text{E/S0}) \simeq 1.7M_\odot/L_\odot$ and $M_*/L_i(\text{Sp}) \simeq 0.9M_\odot/L_\odot$. All the above use the Chabrier IMF (or are scaled to it). Adopting the Salpeter IMF increases these mass-to-light ratios by a factor of ~ 2 .

Measurements of M_*/L_i for the Milky Way and M31, “typical” L^* spiral galaxies, find $M_*/L_I(\text{MW}) = 1.3 - 1.6M_\odot/L_\odot$ (Flynn et al. 2006) or $M_*/L_I(\text{MW}) = 1.4 - 2.0M_\odot/L_\odot$ (McMillan 2011; Flynn et al. 2006), and Tamm et al. (2012) find $M_*/L_i(\text{M31}) \simeq 2.9M_\odot/L_\odot$ for all components of the galaxy combined. The value for M31 is significantly higher than that found for the Milky Way and other spirals above; this may be caused by M31’s relatively red color for a spiral (Tempel et al. 2011). The M_*/L_i values for the Milky Way and M31 seem to indicate a higher M_*/L_i for spirals than found by some of the models above; as a result, we adopt the higher range of values from the sources described, using $M_*/L_i(\text{E/S0}) = 2.5M_\odot/L_\odot$ and $M_*/L_i(\text{Sp}) = 1.3M_\odot/L_\odot$. The results for the stellar fraction discussed below are proportional to the assumed value of M_*/L_i ; using different values, the resulting stellar mass and stellar mass fraction will scale proportionally.

Since M_*/L_i is independent of the Hubble parameter h , we convert the M/L_i ratios presented in the previous section (which were presented in units of h) to the Λ CDM

$h = 0.7$ (thus reducing all M/L_i by 0.7). The total observed mass-to-light ratio — including the BCG and accounting for the total luminosity of the system (§3.2) — is then used to determine f_* as described above. In the top panel of Figure 9 we present the local stellar fraction f_* as a function of radius in units of r/r_{200} . The stellar mass fraction is essentially constant with radius from 0.2 to $40r_{200}$, with a value $f_* \simeq 1.0 \pm 0.4\%$ for all richnesses. Also shown is a horizontal band representing the average stellar mass fraction of the Universe. For this, we use the measured luminosity density of $1.61 \pm 0.05 \times 10^8 h L_\odot \text{Mpc}^{-3}$ (§6), increased by a factor of 1.36 to account for the light from galaxies below our luminosity threshold (§3.2). We combine this with the M_*/L_i for spirals and E/SOs as discussed above to obtain a cosmic mean stellar mass density of $\rho_* = 2.8 \pm 0.2 \times 10^8 M_\odot \text{Mpc}^{-3}$ (for $h = 0.7$), implying $f_{*,\text{cosmic}} = 0.9 \pm 0.1\%$. This is consistent with the mean stellar mass density of $\rho_* \simeq 3.1 \pm 0.5 \times 10^8 M_\odot \text{Mpc}^{-3}$ ($f_* = 0.9\% \pm 0.2\%$ for $\Omega_m = 0.26 \pm 0.02$; §6) found by Muzzin et al. (2013) using the data of Cole et al. (2001); Bell et al. (2003); Baldry et al. (2012).

The middle panel of Figure 9 shows the cumulative stellar fraction f_* within r/r_{200} . The strong influence of the central BCG is clearly seen in the poor groups, as discussed in §3, causing the increase in stellar fraction near the cluster center. At small r/r_{200} , especially in poor groups, the stellar fraction increases as the BCG becomes dominant. On large scales, systems of all richnesses reach the same cumulative stellar fraction of $f_* \simeq 1\%$. In the lower panel of Figure 9, we present the stellar fraction within r_{200b} , the radius at which the interior mean density is 200 times the matter density of the Universe, versus M_{200b} , the mass within r_{200b} . The increasing stellar fraction at lower mass (smaller r_{200b}) reflects the dominance of the central BCG on this scale (§3).

6 Ω_M

The observed mass-to-light ratio on large scales can be used to determine the mass density of the Universe, Ω_m (e.g., Bahcall et al. 1995; Bahcall & Fan 1998, S09A and references therein). Figure 7 presents the observed M/L_i within two large scales (9 and 18.4 h^{-1} Mpc) around all systems, from the poorest groups to the richest clusters (§3). The observed M/L_i within these large scales is independent of the central environment, reaching a representative cosmic value (see also S09A). This mean value, shown by the horizontal band in Figure 7, is $409 \pm 29 h M_\odot/L_\odot$. Combined with the luminosity density of the Universe in the $i^{0.25}$ band for galaxies above $0.19L^*$, $1.61 \pm 0.05 \times 10^8 h L_\odot/\text{Mpc}^3$ (comoving) (S09A), we find $\Omega_m = 0.24 \pm 0.02 b_{M/L}^2$, independent of h . The small bias factor, $b_{M/L}^2$, depends primarily on the bias of the galaxy tracers relative to the underlying mass distribution (see §2). The galaxies used have a low threshold luminosity of $10^{9.5} h^{-2} L_\odot = 0.19L^*$. The bias of such sub- L^* threshold galaxies is $b \simeq 1.05$ (for $\sigma_8 = 0.83$; increasing to 1.09 for $\sigma_8 = 0.8$; Zehavi et al. 2011). We thus find

$$\Omega_m = 0.24 \pm 0.02 \times b_{M/L}^2 = 0.26 \pm 0.02. \quad (4)$$

7 SUMMARY AND CONCLUSIONS

We compare the distribution of mass and light around 132,473 BCG-centered SDSS groups and clusters as a function of scale, from small scales inside clusters to large cosmic scales of nearly $30 h^{-1}$ Mpc, and for different richness environments. The masses are determined from stacked weak gravitational lensing observations and are used to derive the mass-to-light profile, $M/L_i(< r)$; this profile indicates how light traces mass on all scales and in all environments. We summarize our main conclusions below.

1. The $M/L_i(< r)$ profile rises with radius on small scales inside groups and clusters, reflecting the increasing mass-to-light ratio of the central bright BCG galaxy. $M/L_i(< r)$ then flattens to a nearly constant value, showing that light follows mass on large scales. This flattening to a nearly constant M/L_i ratio begins at relatively small scales of only a few hundred kpc inside clusters and remains nearly constant to the largest cosmic scales of $\sim 30 h^{-1}$ Mpc; this is especially so when accounting for the varying stellar population age as a function of local density (see #3 below). This indicates that light follows mass on all scales (above ~ 300 kpc) and in all environments, even inside clusters. The rise to the flat constant value in the cumulative $M/L_i(< r)$ function is considerably slower in poor groups because they are dominated by light from the central BCG galaxy (see #2 below).

2. The luminosity of the BCG galaxy increases with cluster richness, but its dominance relative to the total cluster luminosity decreases with richness. This decreasing trend of $L_{\text{BCG}}/L_{\text{cluster}}$ with cluster richness affects the cumulative M/L_i profile in the central regions of groups and clusters, causing the slower increase of $M/L_i(< r)$ with radius for poor groups, but reaching a constant M/L_i ratio on very small scales of ~ 300 kpc in rich clusters. The decreasing dominance of the BCG with richness suggests that the growth of the central BCG is less efficient than the growth of the cluster as a whole. Clusters, which evolve by merging and accretion of poorer systems, grow faster than do their central BCG galaxies (also by merging and accretion).

3. The small trends observed in the $M/L_i(< r)$ profile outside the central BCG regions — a slowly decreasing M/L_i with radius and richness — are shown to be consistent with the varying stellar population as a function of density, following the density-morphology relation. This stellar population trend results in a slowly decreasing M/L_i with radius due to the increasing population of young spiral galaxies, which have lower M/L_i than ellipticals, before flattening to a constant cosmic value on larger scales. This indicates that stars, which account for only a few percent of the total mass, trace the total mass remarkably well. The dark matter in the Universe thus follows light, and especially stellar mass, on all scales above a few hundred kpc.

4. We determine the stellar mass fraction as a function of environment and scale, $f_* = M_*/M(r/r_{200})$. We find that the stellar mass fraction is nearly constant on all scales and all environments above few hundred kpc, with $f_* \simeq 1.0 \pm 0.4\%$. This fraction is consistent with the cosmic stellar mass fraction. The fact that stars follow mass so well is the main reason why light traces mass on all these scales.

5. We show that most of the dark matter in the Universe may be located in large dark matter halos around individual

galaxies (~ 300 kpc for L^* galaxies). The mass and mass-to-light ratio of groups, clusters, and large scale structure is consistent with being contributed by the mass of individual galaxies, including their large dark matter halos (which may be stripped off inside the dense regions of clusters), plus the additional intergalactic/intracluster gas. The mass from individual galaxies, plus gas, appear to be consistent with the entire observed M/L profile on all scales and in all environments (Fig. 8). This suggests that most of the dark matter in the Universe may be located in the large halos of individual galaxies; groups, clusters, and large scale structure are simply made-up by this dark matter; they do not contain significantly more dark matter (relative to light) than do the individual galaxies.

6. The constant M/L_i ratio on large scales represents the universal mass-to-light ratio. This corresponds to a mass-density parameter of $\Omega_m = 0.24 \pm 0.02 \times b_{M/L}^2 = 0.26 \pm 0.02$ (where the small galaxy bias factor is ~ 1.05).

ACKNOWLEDGMENTS

We thank the referee for the helpful comments on the paper. A. K. acknowledges support from an NSF graduate research fellowship.

REFERENCES

- Adelman-McCarthy J. K. et al., 2006, *ApJS*, 162, 38
Bahcall N. A., Cen R., Davé R., Ostriker J. P., Yu Q., 2000, *ApJ*, 541, 1
Bahcall N. A., Comerford J. M., 2002, *ApJ*, 565, L5
Bahcall N. A., Dong F., Hao L., Bode P., Annis J., Gunn J. E., Schneider D. P., 2003, *ApJ*, 599, 814
Bahcall N. A., Fan X., 1998, *ApJ*, 504, 1
Bahcall N. A., Lubin L. M., Dorman V., 1995, *ApJ*, 447, L81
Baldry I. K. et al., 2012, *MNRAS*, 421, 621
Bamford S. P. et al., 2009, *MNRAS*, 393, 1324
Bell E. F., McIntosh D. H., Katz N., Weinberg M. D., 2003, *ApJS*, 149, 289
Blanton M. R. et al., 2001, *AJ*, 121, 2358
Blanton M. R. et al., 2003, *ApJ*, 592, 819
Blanton M. R., Roweis S., 2007, *AJ*, 133, 734
Boylan-Kolchin M., Bullock J. S., Sohn S. T., Besla G., van der Marel R. P., 2013, *ApJ*, 768, 140
Brimioulle F., Seitz S., Lerchster M., Bender R., Snigula J., 2013, *MNRAS*, 432, 1046
Bruzual G., Charlot S., 2003, *MNRAS*, 344, 1000
Carlberg R. G., Yee H. K. C., Ellingson E., Abraham R., Gravel P., Morris S., Pritchet C. J., 1996, *ApJ*, 462, 32
Cen R., Ostriker J. P., 2006, *ApJ*, 650, 560
Cole S. et al., 2001, *MNRAS*, 326, 255
Courteau S., van den Bergh S., 1999, *AJ*, 118, 337
Cox A. N., 2000, *Allen's astrophysical quantities*
Davis M., Tonry J., Huchra J., Latham D. W., 1980, *ApJ*, 238, L113
Dressler A., 1980, *ApJ*, 236, 351
Dressler A. et al., 1997, *ApJ*, 490, 577
Flynn C., Holmberg J., Portinari L., Fuchs B., Jahreiß H., 2006, *MNRAS*, 372, 1149
Gallazzi A., Bell E. F., 2009, *ApJS*, 185, 253
Gallazzi A., Charlot S., Brinchmann J., White S. D. M., Tremonti C. A., 2005, *MNRAS*, 362, 41
Girardi M., Borgani S., Giuricin G., Mardirossian F., Mezzetti M., 2000, *ApJ*, 530, 62
Graves G. J., Faber S. M., 2010, *ApJ*, 717, 803
Guo Q., White S., Li C., Boylan-Kolchin M., 2010, *MNRAS*, 404, 1111
Hansen S. M., McKay T. A., Wechsler R. H., Annis J., Sheldon E. S., Kimball A., 2005, *ApJ*, 633, 122
Hansen S. M., Sheldon E. S., Wechsler R. H., Koester B. P., 2009, *ApJ*, 699, 1333
Johnston D. E. et al., 2007, *ArXiv e-prints*
Kauffmann G. et al., 2003, *MNRAS*, 341, 33
Koester B. P. et al., 2007a, *ApJ*, 660, 239
Koester B. P. et al., 2007b, *ApJ*, 660, 221
Kuntschner H. et al., 2010, *MNRAS*, 408, 97
Lagattuta D. J. et al., 2010, *ApJ*, 716, 1579
Leauthaud A. et al., 2012, *ApJ*, 746, 95
Li Y.-S., White S. D. M., 2008, *MNRAS*, 384, 1459
Lin Y.-T., Mohr J. J., Stanford S. A., 2004, *ApJ*, 610, 745
Mandelbaum R. et al., 2008, *MNRAS*, 386, 781
McMillan P. J., 2011, *MNRAS*, 414, 2446
Montero-Dorta A. D., Prada F., 2009, *MNRAS*, 399, 1106
Muzzin A. et al., 2013, *ApJ*, 777, 18
Niederste-Ostholt M., Strauss M. A., Dong F., Koester B. P., McKay T. A., 2010, *MNRAS*, 405, 2023
Ostriker J. P., Peebles P. J. E., Yahil A., 1974, *ApJ*, 193, L1
Peebles P. J. E., 1989, *ApJ*, 344, L53
Phelps S., Nusser A., Desjacques V., 2013, *ApJ*, 775, 102
Popesso P., Biviano A., Böhringer H., Romaniello M., 2007, *A&A*, 464, 451
Postman M., Geller M. J., 1984, *ApJ*, 281, 95
Prochaska J. X., Hennawi J. F., Simcoe R. A., 2013, *ApJ*, 762, L19
Proctor R. N., Sansom A. E., 2002, *MNRAS*, 333, 517
Rasheed B., Bahcall N., Bode P., 2010, *PNAS*, 108, 3487
Roediger J. C., Courteau S., MacArthur L. A., McDonald M., 2011, *MNRAS*, 416, 1996
Rozo E. et al., 2009, *ApJ*, 699, 768
Rubin V. C., Thonnard N., Ford, Jr. W. K., 1978, *ApJ*, 225, L107
Seljak U., Warren M. S., 2004, *Monthly Notices of the Royal Astronomical Society*, 355, 129
Sheldon E. S. et al., 2009a, *ApJ*, 703, 2232
Sheldon E. S. et al., 2009b, *ApJ*, 703, 2217
Sheth R. K., Tormen G., 1999, *MNRAS*, 308, 119
Spergel D. N. et al., 2007, *ApJS*, 170, 377
Tal T., van Dokkum P. G., 2011, *ApJ*, 731, 89
Tamm A., Tempel E., Tenjes P., Tihhonova O., Tuvikene T., 2012, *A&A*, 546, A4
Tegmark M. et al., 2004, *ApJ*, 606, 702
Tempel E., Tuvikene T., Tamm A., Tenjes P., 2011, *A&A*, 526, A155
Thomas D., Maraston C., Bender R., Mendes de Oliveira C., 2005, *ApJ*, 621, 673
Tinker J. L. et al., 2012, *ApJ*, 745, 16
Tinker J. L., Weinberg D. H., Zheng Z., Zehavi I., 2005, *ApJ*, 631, 41
Trager S. C., Faber S. M., Worthey G., González J. J., 2000, *AJ*, 119, 1645

- van der Marel R. P., Fardal M., Besla G., Beaton R. L.,
Sohn S. T., Anderson J., Brown T., Guhathakurta P.,
2012, *ApJ*, 753, 8
van der Wel A., 2008, *ApJ*, 675, L13
York D. G. et al., 2000, *AJ*, 120, 1579
Yoshino A., Ichikawa T., 2008, *PASJ*, 60, 493
Zehavi I. et al., 2011, *ApJ*, 736, 59
Zhu G., Blanton M. R., Moustakas J., 2010, *ApJ*, 722, 491
Zibetti S., White S. D. M., Schneider D. P., Brinkmann J.,
2005, *MNRAS*, 358, 949
Zwicky F., 1937, *ApJ*, 86, 217